APPLIED SCIENCES AND ENGINEERING

Biomimetic anisotropic polymeric nanoparticles coated with red blood cell membranes for enhanced circulation and toxin removal

Elana Ben-Akiva[1,2], Randall A. Meyer[1], Hongzhe Yu[1], Jonathan T. Smith[1], Drew M. Pardoll[2,3], Jordan J. Green[1,2]*

The design of next-generation nanobiomaterials requires precise engineering of both physical properties of the core material and chemical properties of the material's surface to meet a biological function. A bio-inspired modular and versatile technology was developed to allow biodegradable polymeric nanoparticles to circulate through the blood for extended periods of time while also acting as a detoxification device. To mimic red blood cells, physical and chemical biomimicry are combined to enhance the biological function of nanomaterials in vitro and in vivo. The anisotropic shape and membrane coating synergize to resist cellular uptake and reduce clearance from the blood. This approach enhances the detoxification properties of nanoparticles, markedly improving survival in a mouse model of sepsis. The anisotropic membrane-coated nanoparticles have enhanced biodistribution and therapeutic efficacy. These biomimetic biodegradable nanodevices and their derivatives have promise for applications ranging from detoxification agents, to drug delivery vehicles, and to biological sensors.

INTRODUCTION

Biomaterial-based devices can have enhanced therapeutic function through biomimicry of naturally occurring structures. For example, as red blood cells (RBCs) enable long-term circulation in the blood, we hypothesized that biologically inspired nanoparticles that mimicked both chemical and physical properties of RBCs could also have enhanced blood circulation. Cell membrane coating can be used to enhance the delivery properties of nanoparticles by mimicking the functionality of various cell types and extending blood circulation half-life (*1*–*5*). However, all previous work has used spherical nanoparticles and thus lacks an important aspect of bio-inspired design (*6*). Particulate shape is a critical design parameter as it has been previously shown to affect the drug delivery properties of therapeutics (*7*–*9*). The combined roles of physical biomimicry (RBC-mimetic shape and enhanced surface area–to–volume ratio) and chemical biomimicry (RBC membrane–derived surface coating) are investigated here to improve the blood circulation and detoxification properties of biodegradable poly(lactic-*co*-glycolic acid) (PLGA) nanoparticles.

Coating particles with naturally derived cell membranes is a promising approach to biomimetic particle engineering that confers particles with the properties of a specific cell type. Many biomaterials have been synthetically designed to mimic cell membranes, but these bottom-up engineering approaches are unable to entirely recapitulate the complex structure and protein composition of cell membranes (*10*–*13*). The top-down design approach of coating particles with naturally derived cell membranes can circumvent this obstacle. In addition to a biomimetic surface, shape is an important particle characteristic that could enhance the biomimetic nature and drug delivery properties of nanoparticles. Anisotropic nanoparticles are superior to spherical particles with respect to biodistribution and targeted cell interactions (*9*, *14*, *15*). They have greater resistance to nonspecific cellular elimination upon systemic administration compared to spherical particles, which would augment the stealth nature of membrane-coated particles (*14*, *16*, *17*). Anisotropic particles also have increased targeted interactions with cells due to a higher surface area–to–volume ratio (*18*, *19*). Cell membranes undergo frequent shape remodeling, and both cell membranes and membrane vesicles often exhibit anisotropic shapes and varying degrees of curvature (*20*, *21*). Therefore, we hypothesized that cell membrane vesicles may be able to alter their shape as a result of interactions with the surface of anisotropic nanoparticles to successfully coat them in a similar manner to how spherical nanoparticles have been coated. While very small anisotropic nanoparticles may have difficulties being coated, the nanoparticles used in these experiments (>200 nm) have physical properties that lead to successful coating.

An important characteristic of systemically administered biomaterials is the capability to avoid immediate clearance from the bloodstream and persist for longer periods of time in circulation. Typically, this is achieved by functionalizing the particle surface with a biocompatible material, most commonly poly(ethylene glycol) (PEG), that reduces particle recognition and uptake by the reticuloendothelial system (RES), and various particle engineering strategies have been applied to use and enhance the "stealth" ability of PEG (*22*–*25*). RBC membrane–coated nanoparticles have been developed in an effort to mimic the long circulation time of natural RBCs, and they serve as an alternative strategy to engineer stealth nanoparticles that have the potential to be more effective than current approaches (*1*). It has also been shown that nonspherical particles can successfully evade elimination, contributing to longer circulation times and enhanced therapeutic efficacy (*14*). On the basis of these previous studies, we hypothesized that particle anisotropy could synergize with the biomimetic RBC membrane coating to achieve a more favorable pharmacokinetic profile and greater therapeutic efficacy.

[1]Departments of Biomedical Engineering, Materials Science and Engineering, Chemical and Biomolecular Engineering, and Oncology, Translational Tissue Engineering Center, Institute for Nanobiotechnology, Johns Hopkins School of Medicine, 400 N Broadway, Smith Building 5017, Baltimore, MD 21231, USA. [2]Bloomberg-Kimmel Institute for Cancer Immunotherapy, Sidney Kimmel Comprehensive Cancer Center, Johns Hopkins University School of Medicine, Baltimore, MD 21231, USA. [3]Departments of Oncology, Medicine, Pathology and Molecular Biology and Genetics, Johns Hopkins University School of Medicine, Baltimore, MD 21231, USA.
*Corresponding author. Email: green@jhu.edu

RESULTS

Fabrication and characterization of RBC membrane–coated PLGA nanoparticles

To fabricate anisotropic PLGA nanoparticles, spherical nanoparticles were first synthesized by single emulsion and then stretched using an automated thin-film stretching protocol (Fig. 1) (*26*). Spherical particles were cast into thin plastic films that were stretched at 90°C, above the glass transition temperature of PLGA. Films were stretched 2-fold in one dimension (unless otherwise specified) or 1.5-fold in two dimensions to generate prolate or oblate ellipsoidal nanoparticles, respectively. Following retrieval of the particles from the thin films, the particles were fused with processed nanovesicles from fresh RBC membranes to yield a biomimetic lipid membrane on the surface of the particle derived from a natural RBC.

Upon coating of the particles with the RBC membrane, the samples were imaged under transmission electron microscopy (TEM) to confirm the presence of the membrane coating on the surface of the particle (Fig. 2A). The particles were successfully deformed into nonspherical shapes as has been previously shown using this method, and the synthesized particles were approximately 240 nm in size (*14*). The membrane-coated nanoparticles had a halo around the surface of the particle that was not present on the noncoated samples. This halo is similar to previous reported results that demonstrated the presence of a membrane halo around the surface of the spherical nanoparticles upon RBC membrane coating (*1*, *3*, *27*).

To further confirm the presence of an RBC membrane coating on the anisotropic nanoparticles, the spherical nanoparticles were sized before and after coating by dynamic light scattering (DLS) (Fig. 2B). The coated nanoparticles exhibited an increase in diameter of 17.2 nm, which is approximately consistent with what would be expected based on a reported RBC membrane thickness of about 8 nm (*28*). The zeta potential of the spherical particles was also measured to determine the presence of the RBC membrane coating (Fig. 2C). Uncoated spherical nanoparticles had a zeta potential of −35.9 mV, on average. However, the coated spherical nanoparticles had a zeta potential of −28.3 mV, similar to the zeta potential of the RBC-derived membrane vesicles, which was −27.2 mV on average. These changes in both size and surface charge confirm that the spherical nanoparticles were successfully coated with RBC membranes.

The presence of CD47 on the surface of the particle was also confirmed to assess the functional potential of the particles to evade macrophage uptake. CD47 is a "marker of self" receptor present on the surface of RBCs that binds to the signal regulatory protein α receptor on macrophages and inhibits phagocytosis of RBCs (*29*). As a result, the presence of CD47 on nanoparticles could allow them to escape elimination by macrophages in the RES and persist for a longer time in circulation. Synthetic CD47-based peptides have been found to enhance biodistribution of systemically administered biomaterials by inhibiting phagocytosis (*10*). Particles were stained with a fluorescent antibody against CD47, and there was a sixfold increase in CD47 antibody signal on coated particles of all shapes relative to an uncoated control (Fig. 2D). Together, this evidence indicates that spherical and nonspherical nanoparticles were successfully coated with biomimetic RBC-derived membranes.

In vitro phagocytic uptake of nanoparticles

As an in vitro model of RES clearance, phagocytic uptake of the coated and uncoated nanoparticles by murine macrophages (RAW 264.7)

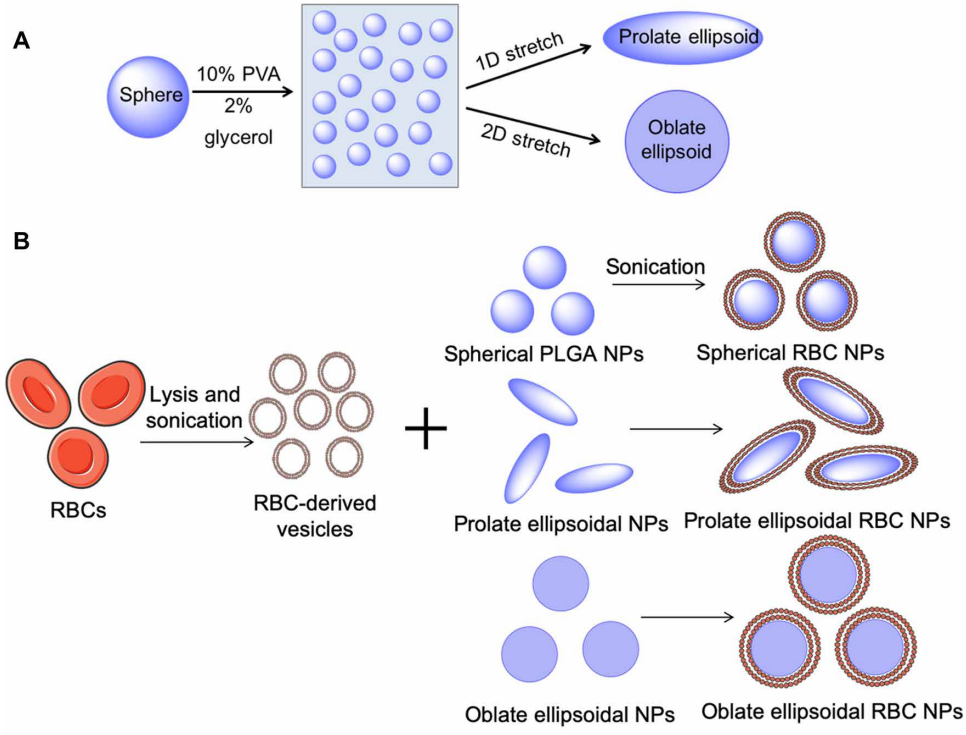

Fig. 1. Schematic of anisotropic nanoparticle fabrication and RBC membrane coating. (**A**) Spherical PLGA nanoparticles (NPs) were synthesized and cast into a thin plastic film of 10% polyvinyl alcohol (PVA) and 2% glycerol. Particles were then stretched under heat in one or two dimensions (2D) to generate prolate or oblate ellipsoidal particles, respectively. (**B**) RBCs underwent hypotonic lysis and were then sonicated to generate sub–200 nm vesicles. RBC-derived vesicles were then coated onto PLGA nanoparticles of all shapes under sonication.

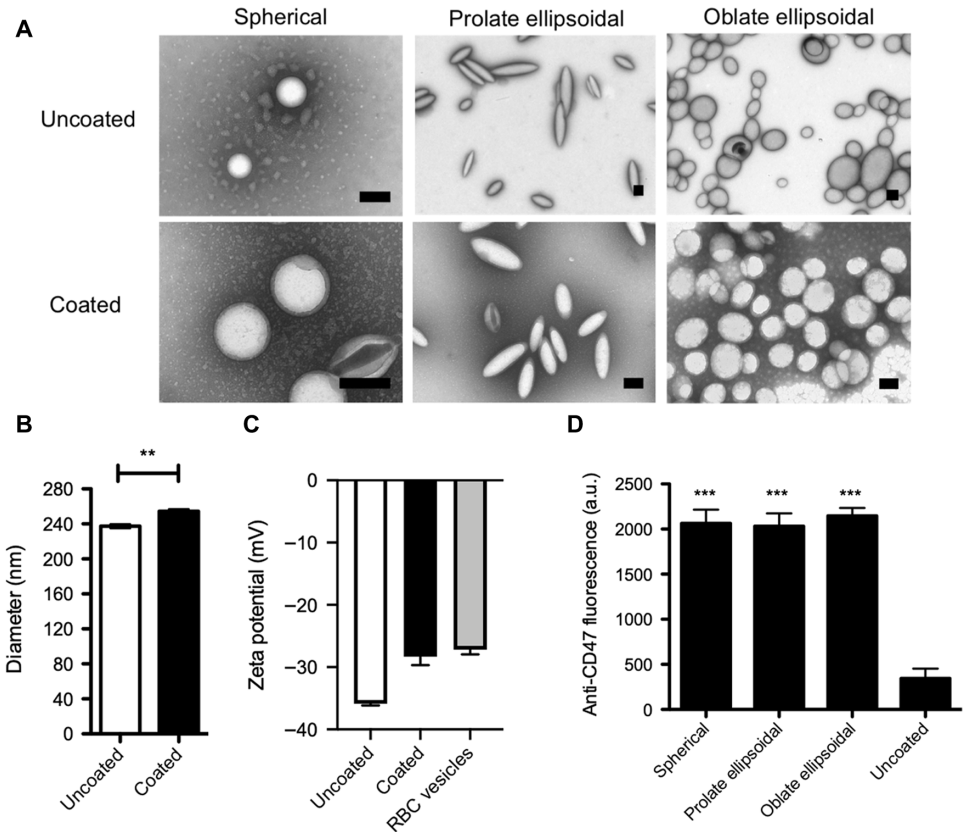

Fig. 2. Nanoparticle characterization. (**A**) Uncoated and RBC-coated spherical, prolate ellipsoidal, and oblate ellipsoidal nanoparticles were imaged by TEM, and coated particles were found to have a halo around the particle core that was not present on uncoated particles. Scale bars. 200 nm. (**B**) Dynamic light scattering (DLS) analysis of coated versus uncoated spherical nanoparticles indicates an increase in diameter of 17.2 nm for coated nanoparticles. (**C**) Zeta potential measurements of uncoated and coated spherical nanoparticles compared to RBC vesicles. (**D**) RBC membrane–coated spherical, prolate ellipsoidal, and oblate ellipsoidal particles and uncoated spherical particles were stained with fluorescent anti-CD47. Data are shown as means ± SEM ($n = 4$ replicates). $^{**}P < 0.01$ and $^{***}P < 0.001$. Student's t test was used to assess the difference in size between coated and uncoated particles, and one-way analysis of variance (ANOVA) with post hoc Dunnett's test was used to compare anti-CD47 staining to the uncoated control. a.u., arbitrary units.

was evaluated. Nanoparticle uptake was assessed quantitatively by flow cytometry (Fig. 3A and fig. S1, A and B) and qualitatively by confocal microscopy (Fig. 3B and fig. S1C). Both altering the nanoparticle shape and imparting a biomimetic RBC membrane surface to the particle reduced cellular uptake by macrophages. This apparent difference in cellular uptake was confirmed by flow cytometry analysis of macrophages that had been incubated with fluorescent particles for 1 (fig. S1b) or 4 hours (Fig. 3A). There were no significant differences between uptake levels for cells incubated with particles for 30 min (fig. S1A), possibly due to the relatively low uptake at this time point. At the 4-hour time point, the membrane coating resulted in a 30 to 50% reduction in cellular uptake compared to uncoated particles (Fig. 3A). There was an additional 30 to 40% reduction in cellular uptake attributed to the anisotropic shape of the nanoparticle. Combined, these two parameters resulted in a 50 to 60% reduction in cellular uptake of anisotropic coated nanoparticles, compared to spherical uncoated nanoparticles. Furthermore, this trend of both parameters working together to achieve cell uptake reduction was apparent across multiple doses of particles tested with the macrophages. It has been previously found that both shape and membrane coating can reduce cellular uptake individually (*1*, *17*, *30*). However, this study demonstrates that the physical biomimicry of the particle core and the chemical biomimicry of the particle surface can synergize to achieve a superior resistance to macrophage elimination.

In vivo nanoparticle clearance and biodistribution

The in vivo potential for a more favorable biodistribution of anisotropic RBC membrane–coated nanoparticles was also assessed. Following the in vitro finding of reduced nonspecific cellular elimination of anisotropic coated particles, it was expected that this result would translate in vivo and that both the nonspherical shape and the biomimetic RBC membrane coating could contribute to enhancement of nanoparticle pharmacokinetics. Nanoparticles of spherical, prolate ellipsoidal, and oblate ellipsoidal shape were synthesized with a hydrophobic near-infrared (IR) fluorophore encapsulated in the particle core for fluorescence analysis of nanoparticles in the bloodstream. The particles, with or without an RBC membrane coating, were injected intravenously via retroorbital injection, and blood was sampled at 15, 30, and 45 min and 2, 4, and 24 hours after particle administration to evaluate systemic nanoparticle concentration. All particle concentrations decayed over time exponentially (Fig. 4a) and, for all particle shapes, incorporation of RBC membranes resulted in a slower exponential decay compared to respective uncoated controls. The experimental data were fit to a single-phase exponential decay curve

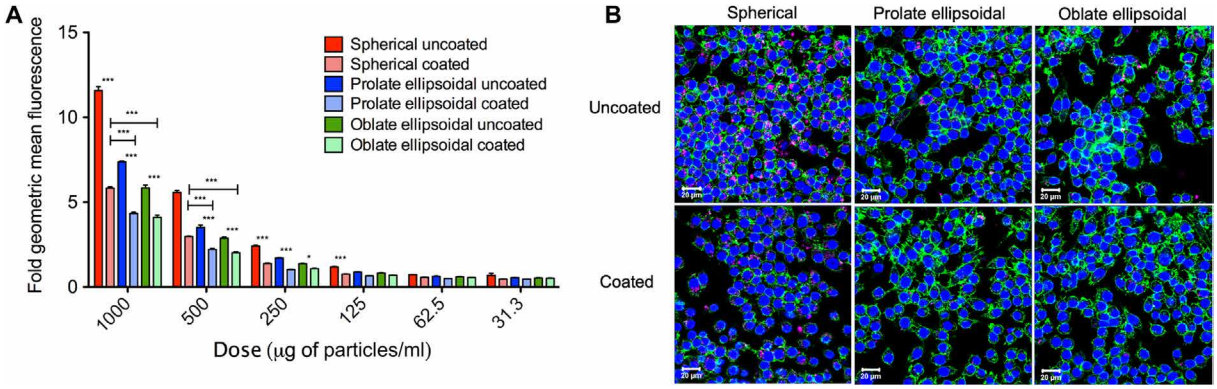

Fig. 3. In vitro macrophage uptake of nanoparticles. (**A**) Fluorescent nanoparticles were incubated with RAW 264.7 macrophages for 4 hours, and uptake was analyzed by flow cytometry. Relative uptake, as measured by geometric mean fluorescence normalized to untreated cells, was significantly reduced as a result of anisotropy and membrane coating. (**B**) Macrophage uptake of nanoparticles (pink) was visualized by confocal imaging and found to be reduced for anisotropic coated particles. Macrophages were stained for nuclei (blue) and actin (green). Scale bars, 20 μm. Data are shown as means ± SEM ($n = 4$ replicates). Statistics were performed by a two-way ANOVA with Bonferroni's posttests (*$P < 0.05$ and ***$P < 0.001$).

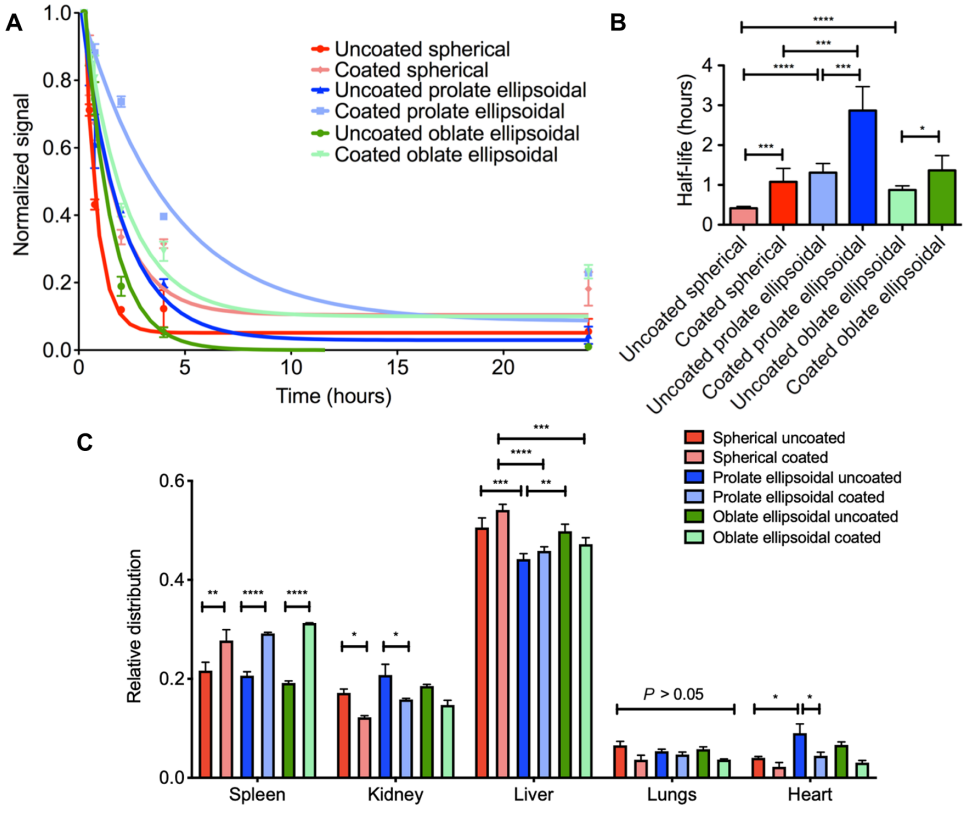

Fig. 4. In vivo clearance and biodistribution of nanoparticles. (**A**) Blood elimination of nanoparticles following intravenous administration as assessed by fluorescence readings of the blood sample (dots) and fit to a single exponential decay model (lines). (**B**) Particle bloodstream half-life was derived from the exponential fit of blood decay curves and was increased for RBC membrane–coated particles and prolate ellipsoidal particles. (**C**) Mice were euthanized after 24 hours, and organs were dissected out and imaged. Data are shown as means ± SEM ($n = 3$ mice per group). Statistics were performed by a one-way ANOVA with post hoc Tukey's test (*$P < 0.05$, **$P < 0.01$, ***$P < 0.001$, and ****$P < 0.0001$).

to derive systemic half-life information for the particle samples. The half-life of the coated nanoparticles significantly exceeded that of the uncoated particles (Fig. 4B). For example, the uncoated spherical nanoparticles had an average half-life of 24.6 min, whereas the coated spherical nanoparticles had an average half-life of 64.8 min, a 2.63-fold increase. Furthermore, the prolate ellipsoidal shape resulted in a superior half-life compared to both the spherical and oblate ellipsoidal shapes, with coated prolate ellipsoidal nanoparticles having a half-life of 171.6 min compared to 82.0 min for coated oblate ellipsoidal particles and 64.8 min for coated spherical particles. These data suggest

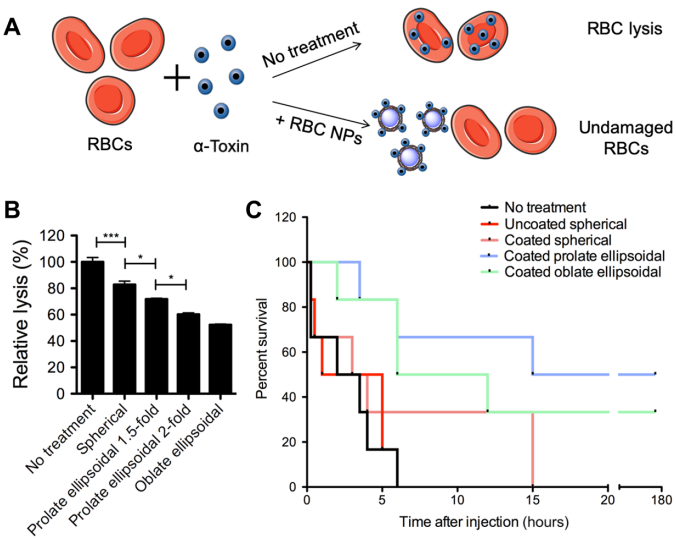

Fig. 5. Anisotropic RBC membrane–coated nanoparticles as detoxification treatment. (**A**) Schematic of mechanism of RBC coated nanoparticles (NPs) as detoxification treatment. RBC NPs neutralize alpha toxin by binding toxin that would otherwise bind the body's RBCs and cause lysis. (**B**) In vitro evaluation of hemolytic toxin absorption by RBC-coated nanoparticles. The anisotropic particles were able to absorb significantly more alpha toxin as evidenced by reduction in relative lysis. Data are shown as means ± SEM ($n = 4$ replicates), and one-way ANOVA with post hoc Tukey's test was used to compare across groups. (**C**) Survival following intravenous alpha toxin administration followed by nanoparticle administration ($n = 6$ mice per group). Mice receiving prolate ellipsoidal RBC-coated nanoparticles had a significant long-term survival benefit compared to spherical coated nanoparticles ($P = 0.0481$), and both anisotropic particle groups had a significant survival benefit over uncoated particles ($P = 0.0105$ for coated prolate ellipsoidal, $P = 0.0169$ for coated oblate ellipsoidal) by log rank (Mantel-Cox) test. *$P < 0.05$, **$P < 0.01$, ***$P < 0.001$, and ****$P < 0.0001$.

that the combination of biomimetic physical and chemical particle properties could result in an approximately sixfold increase in half-life.

With respect to the oblate ellipsoidal particles, although in vitro results were favorable with respect to resistance to cellular elimination, the in vivo effect was not as marked as anticipated. We hypothesize that the prolate ellipsoidal particles may be more hydrodynamically efficient in the blood than the oblate ellipsoidal particles, leading to the superior half-life of the prolate ellipsoidal particles in vivo.

At 24 hours after administration, the major nonbowel organs (spleen, kidney, liver, lung, and heart) were dissected out to analyze fluorescence and determine the ultimate distribution of the particles following systemic administration (Fig. 4C). Organ distribution of the particles was also assessed at 4 hours (fig. S2A) and 72 hours (fig. S2B). At 4 and 24 hours, the major centers of accumulation of the particles were the spleen and liver, as expected based on previous studies evaluating nanoparticle biodistribution (*14*). There were some statistically significant differences in organ distribution at 4 and 24 hours. At 24 hours, the coated particles for all shapes accumulated more in the spleen, while there was more signal from the dye in the kidney for the uncoated particles. This could be due to the fact that the uncoated particles are cleared and degraded more quickly than the coated particles, leading to a higher accumulation of the free dye in the kidneys and a lower accumulation of particles in the spleen. Other differences included significantly reduced accumulation of prolate ellipsoidal particles in the liver at 24 hours compared to spherical and oblate ellipsoidal particles and significantly greater accumulation of uncoated prolate ellipsoidal particles in the heart. At 4 hours, there were fewer differences in organ distribution. Spherical coated particles accumulated significantly more in the spleen compared to other groups, while spherical uncoated particles accumulated significantly more in the liver. At 72 hours, there was no statistical difference between any of the particle groups in the relative distribution for each organ, possibly due to significant degradation of the particles by this time point, as evidenced by high accumulation of the near-IR dye in the kidneys. These differences in organ distribution at 4 and 24 hours could be applied for targeting of specific organs. In addition, based on previous results demonstrating that it is possible to incorporate a targeting moiety into the naturally derived membrane, it could be possible to leverage the slower systemic elimination to further target the nanoparticles to a desired site, such as a tumor for cancer drug delivery (*31*).

Detoxification capability of anisotropic RBC membrane–coated nanoparticles

The combination of anisotropic shape and RBC membrane coating was investigated for potential enhancement in a therapeutic application. The biomimetic particles were used as a nanodevice to absorb the bacterial pore-forming toxin, alpha toxin, from the blood (Fig. 5A). In this system, the membrane-coated nanoparticles function as a decoy to absorb the hemolytic toxin from systemic circulation before it can cause irreversible damage to the host's RBCs. Current detoxification treatments need to be customized for each disease based on the molecular structure of the toxin, but in contrast, these nanodevices can work nonspecifically by absorbing toxin to their membrane coating, which would be useful for treating exposure to a variety of toxins (*32*). This model has previously been used with spherical nanoparticles, and we were interested to assess how the anisotropic particle shape could influence alpha toxin absorption capabilities (*32*).

To assess the impact of shape alone (without the complicating factor of in vivo pharmacokinetics), an in vitro model of alpha toxin absorption was used. Alpha toxin was coincubated with coated spherical particles, prolate ellipsoidal particles of two different degrees of stretch, and oblate ellipsoidal particles for 30 min. After a 30-min incubation, fresh RBCs were added to determine the toxicity of the mixture by absorption-based measurements of hemolysis. There was a significantly lower rate of hemolysis in the coated anisotropic particle samples compared to the spherical nanoparticles (Fig. 5B). This is likely due to the fact that the anisotropic particles have a greater surface area–to–volume ratio than the spherical particles (*33*). With greater surface area, there would be more available RBC membrane to serve as a decoy to absorb the alpha toxin. This hypothesis is supported by the fact that the relative hemolysis approximately scaled with particle surface area (fig. S3). For example, as the degree of stretching increased from 1.5- to 2-fold for the prolate ellipsoidal particles, which would result in an increase in surface area of approximately 1.1-fold, the degree of hemolysis decreased by about the same factor. When normalized to the surface area, the prolate ellipsoidal twofold stretched and oblate ellipsoidal particles still have slightly increased efficacy in reducing lysis compared to spherical particles. This suggests that, in addition to increased surface area, there may be other characteristics of the anisotropic nanoparticles that enhance their toxin neutralization capability in vitro.

For example, perhaps the larger radius of curvature of the anisotropic nanoparticles allows them to bind toxin more effectively.

Following these favorable in vitro results, the detoxification potential of the anisotropic nanoparticles in vivo was evaluated. To accomplish this, a lethal dose of alpha toxin was administered intravenously to mice. After a 2-min delay, coated spherical, prolate ellipsoidal, or oblate ellipsoidal nanoparticles were administered, as well as an uncoated spherical particle control or no particle treatment (n = 6 mice per group). The survival of the mice was then tracked to determine the detoxification capabilities of the nanoparticles. The mice in the control group had a median survival of 2.75 hours, and there was no statistical improvement in survival by treatments with uncoated particles or spherical coated particles compared to the untreated control (Fig. 3C). However, there was a marked and statistically significant improvement in survival with administration of the anisotropic nanoparticles, both oblate and prolate ellipsoidal. In addition, approximately 50% of the prolate ellipsoidal treated and 33% of the oblate ellipsoidal treated mice were found to be healthy 1 week after particle administration.

Although the oblate ellipsoidal particles have a greater surface area than the prolate ellipsoidal particles and mediated a greater reduction in hemolysis in vitro, they led to a smaller improvement in survival in vivo compared to the prolate ellipsoidal particles. This is likely due to the difference in biodistribution in vivo, as coated prolate ellipsoidal nanoparticles have a significantly longer half-life in the bloodstream than coated oblate ellipsoidal nanoparticles (Fig. 2D). Overall, these results align with the enhanced activity of anisotropic nanoparticles in the in vitro test for alpha toxin absorption, which may have been enhanced by the reduced systemic elimination of the anisotropic coated nanoparticles. Thus, the anisotropic RBC membrane–coated nanoparticle has been validated as a potentially stronger treatment than equivalent spherical coated nanoparticles for detoxification of patients with sepsis (*34*).

DISCUSSION

In this work, anisotropic polymeric biodegradable nanoparticles coated with RBC membranes that have a biomimetic shape and surface composition have been developed, and we have successfully demonstrated the utility of these constructs. Spherical, prolate ellipsoidal, and oblate ellipsoidal PLGA nanoparticles were synthesized and coated with RBC membranes adapting previously established protocols for spherical particles (*1*). The anisotropic nanoparticles were successfully coated with RBC membranes despite their increased radius of curvature. Our previous work has shown that anisotropic microparticles can be coated with liposomes with similar efficiency to spherical particles and that the curvature does not significantly affect the fluidity or stability of the membrane coating (*35*). Here, we have shown that anisotropic nanoparticles can similarly be coated with naturally derived cell membranes despite their increased curvature. However, there is evidence that increasing the curvature of membranes on the nanoscale could affect the lipid fluidity of the membrane coating. The effect of particle anisotropy and curvature on the fluidity and stability of the membrane coating are important future areas of investigation in further characterizing anisotropic membrane-coated nanoparticles (*36*).

Through mimicry of both the shape and the surface membrane of RBCs, we have determined that the combination of these two features achieves an enhancement of drug delivery efficacy that neither parameter can successfully attain on its own. The anisotropic shape and membrane coating are able to synergize with respect to in vitro resistance to cellular uptake and in vivo reduction of clearance rate upon systemic administration. The anisotropic nanoparticles coated with RBC membranes are able to superiorly evade elimination by macrophages compared to their spherical, uncoated counterparts. Furthermore, prolate ellipsoidal, coated nanoparticles exhibit reduced rates of systemic elimination upon intravenous administration compared to other particle shapes tested in this study. Last, the utility of these constructs has been demonstrated through the augmentation of their efficacy as a sepsis detoxification therapy. The enhanced pharmacokinetic properties of the anisotropic, coated particle, in conjunction with the increased surface area due to anisotropic shape, resulted in a stronger capability to mediate detoxification of systemically administered bacterial toxin. This platform has the potential to provide a modular and versatile technology for enhancing drug delivery, and continued investigation into the combinations of biomimetic paradigms such as surface chemistry and morphology will undoubtedly yield optimal particle formulations for enhanced biomedical therapeutics.

MATERIALS AND METHODS

Spherical PLGA nanoparticle synthesis

Polymeric nanoparticles were synthesized using single-emulsion techniques as previously described (*14*, *37*). PLGA terminated (38 to 54 kDa, 50:50 lactide:glycolide ratio) (Sigma-Aldrich, St. Louis, MO) was used as the core material for particle synthesis. For macrophage uptake studies, particles were loaded with 1,1′-dioctadecyl-3,3,3′,3′-tetramethylindodicarbocyanine perchlorate (DiD; Thermo Fisher Scientific, Waltham, MA) at a 0.2% (w/w) ratio to the polymer. For in vivo biodistribution studies, particles were synthesized encapsulating a custom synthesized hydrophobic dye with a 770 excitation/800 emission fluorescence profile (LI-COR Biosciences, Lincoln, NE) at a 2% (w/w) ratio. The PLGA was dissolved at 40 mg/ml in dichloromethane and, for fluorescent particles, the dye was added to the polymer solution. Five milliliters of the polymer solution was then emulsified in 50 ml of 1% polyvinyl alcohol (PVA) solution using a VCX 750 sonicator (Sonics & Materials Inc., Newtown, CT) set to 60% amplitude for 2 min. The resulting emulsification was poured into 100 ml of a 0.5% PVA solution on a magnetic stir plate at 500 rpm, and the particles were allowed to harden for at least 4 hours. The particles were centrifuged at 3000*g* for 5 min to pellet out microparticles. The supernatant was collected and washed three times with deionized water at 40,000*g* for 15 min, frozen, and lyophilized.

Anisotropic PLGA nanoparticle fabrication

PLGA nanoparticles were deformed into prolate or oblate ellipsoidal particles using thin-film stretching methods as has been previously reported (*37*, *38*). Particles were suspended at a concentration of 2.5 mg/ml in a 10% PVA and 2% glycerol solution. The particles were then deposited into rectangular or square petri dishes to deform the particle in one or two dimensions to make prolate or oblate ellipsoidal particles, respectively. After overnight drying of the films, they were loaded onto an automated thin film stretcher that has been previously designed, and the films were stretched 1.5- or 2-fold in one dimension for prolate ellipsoidal or 1.5-fold in two dimensions for oblate ellipsoidal particles at 90°C (*26*). The films were then cooled to room temperature and removed from the stretcher. The

films were then dissolved in deionized water by vortexing, and the particles were washed three times at 40,000*g* for 15 min with deionized water, frozen, and lyophilized before use.

RBC membrane coating

PLGA nanoparticles were coated with RBC membranes using a combination of previously developed protocols (*1*, *35*). Pathogen-free CD1 (in vitro studies) or C57BL6 (in vivo studies) mouse whole blood was purchased (Innovative Research, Novi, MI). One milliliter of whole blood was centrifuged twice at 800*g* to separate the packed RBCs from the serum and white blood cells. The RBCs were then suspended in 1 ml of a hypotonic lysis buffer of 0.25× phosphate-buffered saline (PBS) and chilled to 4°C. The lysis proceeded for 20 min, and the resulting RBC-derived ghosts were centrifuged twice at 17,000*g* for 5 min and resuspended in 1× PBS. The RBC ghosts were then sonicated in a VCX 750 sonicator with a cup attachment in a glass vial at 50% amplitude for 2 min to prepare vesicles that were sub–200 nm in size. The vesicles were then mixed with 2 mg of nanoparticles and sonicated again at 50% amplitude for 2 min. The particles were then centrifuged at 10,000*g* for 5 min and washed three times in 1× PBS and resuspended via vortexing and trituration.

Characterization of RBC-coated nanoparticles

Nanoparticles coated with RBC membranes were characterized by TEM using a FEI Tecnai 12 TWIN TEM. The membrane-coated nanoparticles were stained in 1% uranyl formate as a negative stain. The particles were also characterized by DLS using a Malvern ZetaSizer (Malvern Instruments, Westborough, MA). The particles were suspended at a concentration of 1 mg/ml in 1× PBS and sized in a low-volume disposable cuvette using recommended machine settings. Zeta potential of the particles was measured using a Malvern ZetaSizer Pro. The particles were suspended at a concentration of 1 mg/ml in deionized water and sized in a disposable folded capillary cell using recommended machine settings. To evaluate the presence of CD47 on the surface of the particle, allophycocyanin-labeled anti-mouse CD47 antibody was used (BioLegend, San Diego, CA). Coated particles and uncoated spherical particles were incubated with a 1:100 dilution of the antibody for 1 hour at 4°C in 1× PBS. Following incubation, the particles were washed three times in 1× PBS at 17,000*g* for 5 min and read on a BioTek Synergy 2 plate reader (BioTek, Winooski, VT).

Evaluation of in vitro macrophage uptake

RAW 264.7 (American Type Culture Collection) murine macrophages were used as a model cell for phagocytic elimination. The cells were cultured in Dulbecco's minimal essential media, high glucose (Life Technologies, Grand Island, NY) supplemented with 10% fetal bovine serum and 1% penicillin/streptomycin. For flow cytometry studies, macrophages were seeded at 30,000 cells per well in a 96-well plate. Particles labeled with DiD dye were added to the macrophages and incubated for 30 min, 1 hour, or 4 hours. After the incubation, the cells were washed three times with PBS. For confocal imaging, after particle incubation and cell washing, the cells were fixed in 10% formalin stabilized with methanol (Sigma-Aldrich, St. Louis, MO) for 15 min. The cells were then washed three times with PBS and stained with Alexa 488 Phalloidin (Life Technologies, Grand Island, NY) and 4′,6-diamidino-2-phenylindole (BioChemica, Darmstadt, Germany) following the manufacturers' protocols. The fixed samples were then visualized using a Zeiss 780 FCS.

Evaluation of in vivo pharmacokinetics

All animal experiments were approved by the Johns Hopkins University Animal Care and Use Committee. Coated or uncoated particles of all three shapes ($n = 3$ mice per group) encapsulating a near-IR hydrophobic dye were suspended at 20 mg/ml in sterile PBS, and 100 μl of the nanoparticle suspension was injected intravenously via retroorbital injection into the right eye of C57BL/6J mice (The Jackson Laboratory; Bar Harbor, ME). Blood samples were then collected retroorbitally from the left eye at 15 min, 30 min, 45 min, 2 hours, 4 hours, and 24 hours following particle administration. The blood samples were then read on the BioTek Synergy 2 plate reader, and the sample fluorescence was normalized to the initial 15-min time point to control for variability in the injection. The fluorescence readings were then fit to a single-phase exponential decay curve in GraphPad 7 Prism, and half-lives were derived from the best fit equations. At 4, 24, or 72 hours after administration, the animals were euthanized, and the liver, spleen, kidney, heart, and lungs were dissected out and imaged on a LI-COR Pearl Impulse Imager. A region of interest was drawn around the area of the organ in the image, and the mean gray value was evaluated in ImageJ. For each animal, these values were then normalized to the total sum of fluorescence signal from all organs combined to derive percent distribution information.

Evaluation of in vitro detoxification activity of nanoparticles

The utility of the anisotropic RBC membrane–coated nanoparticles was assessed by adapting an alpha toxin neutralization assay previously developed by Hu *et al.* (*32*). Alpha toxin (1.5 μg; Sigma-Aldrich, St. Louis, MO) was mixed with 100 μl of the RBC membrane–coated spherical, prolate ellipsoidal, or oblate ellipsoidal nanoparticles at 2 mg/ml for 30 min. Mouse RBCs were centrifuged at 800*g* and resuspended in 1× PBS to remove hemoglobin from the RBC suspension. Following this incubation, 900 μl of 5% mouse RBCs were added to the particle/toxin mixture, and the mixture was incubated for an additional 30 min. Following the 30 min, the particles were centrifuged at 17,000*g* for 5 min to pellet out particles and any intact RBCs. The absorbance of the supernatant at 540 nm was read by plate reader to assess the level of hemolysis in the sample. The absorbance readings were normalized to a sample that did not have any particles to neutralize the toxin.

Evaluation of in vivo detoxification activity of nanoparticles

For in vivo evaluation of anisotropic nanoparticle detoxification activity, a lethal dose of alpha toxin (2.5 μg per mouse) was administered systemically to C57BL/6J mice by retroorbital injection. The nanoparticle treatments were administered 2 min later retroorbitally and consisted of either no treatment, uncoated spherical nanoparticles, coated spherical nanoparticles, coated prolate ellipsoidal nanoparticles, or coated oblate ellipsoidal nanoparticles ($n = 6$ mice per group, 3 mg particles per mouse). The animals were monitored for survival every 30 min for 8 hours following particle injection and every several hours thereafter. Animals that survived past 24 hours were taken to be long-term survivors and were found to be healthy 1 week following the start of the experiment.

Statistics

All experiments were performed with $n = 4$ replicates unless otherwise stated. Bar graphs indicate means ± SEM. n.s. (not significant) indicates $P > 0.05$. *$P < 0.05$, **$P < 0.01$, ***$P < 0.001$, and ****$P < 0.0001$.

All statistics were completed using statistical analysis software modules in GraphPad Prism 8 (GraphPad Software Inc., La Jolla, CA). For particle size measurements, a Student's *t* test was used to assess the difference between coated and uncoated particles. For anti-CD47 staining, a one-way analysis of variance (ANOVA) with post hoc Dunnett's test was used to compare coated samples to the uncoated control. For macrophage uptake studies, a two-way ANOVA with Bonferroni's posttests was performed considering dose and particle type (shape/coating) as variables. For the in vivo biodistribution study, a one-way ANOVA with post hoc Tukey's test was used to compare across groups for half-life and organ biodistribution. For in vitro alpha toxin studies, a one-way ANOVA with post hoc Tukey's test was used to compare across groups. For in vivo alpha toxin studies, a log rank (Mantel-Cox) test was used to assess significance between survival curves. In all cases, differences were considered significant if the *P* value of the test was less than 0.05.

SUPPLEMENTARY MATERIALS

Supplementary material for this article is available at http://advances.sciencemag.org/cgi/content/full/6/16/eaay9035/DC1

View/request a protocol for this paper from *Bio-protocol*.

REFERENCES AND NOTES

1. C.-M. J. Hu, L. Zhang, S. Aryal, C. Cheung, R. H. Fang, L. Zhang, Erythrocyte membrane-camouflaged polymeric nanoparticles as a biomimetic delivery platform. *Proc. Natl. Acad. Sci. U.S.A.* **108**, 10980–10985 (2011).
2. R. H. Fang, C. M. J. Hu, B. T. Luk, W. Gao, J. A. Copp, Y. Tai, D. E. O'Connor, L. Zhang, Cancer cell membrane-coated nanoparticles for anticancer vaccination and drug delivery. *Nano Lett.* **14**, 2181–2188 (2014).
3. C.-M. J. Hu, R. H. Fang, K. C. Wang, B. T. Luk, S. Thamphiwatana, D. Dehaini, P. Nguyen, P. Angsantikul, C. H. Wen, A. V. Kroll, C. Carpenter, M. Ramesh, V. Qu, S. H. Patel, J. Zhu, W. Shi, F. M. Hofman, T. C. Chen, W. Gao, K. Zhang, S. Chien, L. Zhang, Nanoparticle biointerfacing by platelet membrane cloaking. *Nature* **526**, 118–121 (2015).
4. X. Wei, G. Zhang, D. Ran, N. Krishnan, R. H. Fang, W. Gao, S. A. Spector, L. Zhang, T-cell-mimicking nanoparticles can neutralize HIV infectivity. *Adv. Mater.* **30**, 1802233 (2018).
5. A. Parodi, N. Quattrocchi, A. L. van de Ven, C. Chiappini, M. Evangelopoulos, J. O. Martinez, B. S. Brown, S. Z. Khaled, I. K. Yazdi, M. V. Enzo, L. Isenhart, M. Ferrari, E. Tasciotti, Synthetic nanoparticles functionalized with biomimetic leukocyte membranes possess cell-like functions. *Nat. Nanotechnol.* **8**, 61–68 (2013).
6. D. A. Fletcher, R. D. Mullins, Cell mechanics and the cytoskeleton. *Nature* **463**, 485–492 (2010).
7. R. A. Meyer, J. C. Sunshine, J. J. Green, Biomimetic particles as therapeutics. *Trends Biotechnol.* **33**, 514–524 (2015).
8. R. Toy, P. M. Peiris, K. B. Ghaghada, E. Karathanasis, Shaping cancer nanomedicine: The effect of particle shape on the in vivo journey of nanoparticles. *Nanomedicine* **9**, 121–134 (2014).
9. Y. Geng, P. Dalhaimer, S. Cai, R. Tsai, M. Tewari, T. Minko, D. E. Discher, Shape effects of filaments versus spherical particles in flow and drug delivery. *Nat. Nanotechnol.* **2**, 249–255 (2007).
10. P. L. Rodriguez, T. Harada, D. A. Christian, D. A. Pantano, R. K. Tsai, D. E. Discher, Minimal "Self" peptides that inhibit phagocytic clearance and enhance delivery of nanoparticles. *Science* **339**, 971–975 (2013).
11. N. Doshi, A. S. Zahr, S. Bhaskar, J. Lahann, S. Mitragotri, Red blood cell-mimicking synthetic biomaterial particles. *Proc. Natl. Acad. Sci. U.S.A.* **106**, 21495–21499 (2009).
12. M. M. Lashof-Sullivan, E. Shoffstall, K. T. Atkins, N. Keane, C. Bir, P. VandeVord, E. B. Lavik, Intravenously administered nanoparticles increase survival following blast trauma. *Proc. Natl. Acad. Sci. U.S.A.* **111**, 10293–10298 (2014).
13. G. L. Nicolson, The Fluid-Mosaic Model of Membrane Structure: Still relevant to understanding the structure, function and dynamics of biological membranes after more than 40 years. *Biochim. Biophys. Acta* **1838**, 1451–1466 (2014).
14. R. A. Meyer, J. C. Sunshine, K. Perica, A. K. Kosmides, K. Aje, J. P. Schneck, J. J. Green, Biodegradable nanoellipsoidal artificial antigen presenting cells for antigen specific T-cell activation. *Small* **11**, 1519–1525 (2015).
15. S. Barua, J. W. Yoo, P. Kolhar, A. Wakankar, Y. R. Gokarn, S. Mitragotri, Particle shape enhances specificity of antibody-displaying nanoparticles. *Proc. Natl. Acad. Sci. U.S.A.* **110**, 3270–3275 (2013).
16. J. A. Champion, S. Mitragotri, Role of target geometry in phagocytosis. *Proc. Natl. Acad. Sci. U.S.A.* **103**, 4930–4934 (2006).
17. L. Florez, C. Herrmann, J. M. Cramer, C. P. Hauser, K. Koynov, K. Landfester, D. Crespy, V. Mailänder, How shape influences uptake: Interactions of anisotropic polymer nanoparticles and human mesenchymal stem cells. *Small* **8**, 2222–2230 (2012).
18. S. Shukla, F. J. Eber, A. S. Nagarajan, N. A. DiFranco, N. Schmidt, A. M. Wen, S. Eiben, R. M. Twyman, C. Wege, N. F. Steinmetz, The impact of aspect ratio on the biodistribution and tumor homing of rigid soft-matter nanorods. *Adv. Healthc. Mater.* **4**, 874–882 (2015).
19. G. Adriani, M. D. de Tullio, M. Ferrari, F. Hussain, G. Pascazio, X. Liu, P. Decuzzi, The preferential targeting of the diseased microvasculature by disk-like particles. *Biomaterials* **33**, 5504–5513 (2012).
20. T. Kosawada, K. Inoue, G. W. Schmid-Schönbein, Mechanics of curved plasma membrane vesicles: Resting shapes, membrane curvature, and in-plane shear elasticity. *J. Biomech. Eng.* **127**, 229–236 (2004).
21. Z. Shi, T. Baumgart, Dynamics and instabilities of lipid bilayer membrane shapes. *Adv. Colloid Interface Sci.* **208**, 76–88 (2014).
22. J. S. Suk, Q. Xu, N. Kim, J. Hanes, L. M. Ensign, PEGylation as a strategy for improving nanoparticle-based drug and gene delivery. *Adv. Drug Deliv. Rev.* **99**, 28–51 (2016).
23. H. Zhou, Z. Fan, P. Y. Li, J. Deng, D. C. Arhontoulis, C. Y. Li, W. B. Bowne, H. Cheng, Dense and dynamic polyethylene glycol shells cloak nanoparticles from uptake by liver endothelial cells for long blood circulation. *ACS Nano* **12**, 10130–10141 (2018).
24. H. Qi, H. Zhou, Q. Tang, J. Y. Lee, Z. Fan, S. Kim, M. C. Staub, T. Zhou, S. Mei, L. Han, D. J. Pochan, H. Cheng, W. Hu, C. Y. Li, Block copolymer crystalsomes with an ultrathin shell to extend blood circulation time. *Nat. Commun.* **9**, 3005 (2018).
25. Y. Lu, Z. Yue, J. Xie, W. Wang, H. Zhu, E. Zhang, Z. Cao, Micelles with ultralow critical micelle concentration as carriers for drug delivery. *Nat. Biomed. Eng.* **2**, 318–325 (2018).
26. R. A. Meyer, R. S. Meyer, J. J. Green, An automated multidimensional thin film stretching device for the generation of anisotropic polymeric micro- and nanoparticles. *J. Biomed. Mater. Res.* **103**, 2747–2757 (2015).
27. D. Dehaini, X. Wei, R. H. Fang, S. Masson, P. Angsantikul, B. T. Luk, Y. Zhang, M. Ying, Y. Jiang, A. V. Kroll, W. Gao, L. Zhang, Erythrocyte–platelet hybrid membrane coating for enhanced nanoparticle functionalization. *Adv. Mater.* **29**, 1606209 (2017).
28. R. Hochmuth, C. Evans, H. Wiles, J. McCown, Mechanical measurement of red cell membrane thickness. *Science* **220**, 101–102 (1983).
29. P.-A. Oldenborg, A. Zheleznyak, Y. F. Fang, C. F. Lagenaur, H. D. Gresham, F. P. Lindberg, Role of CD47 as a marker of self on red blood cells. *Science* **288**, 2051–2054 (2000).
30. G. Sharma, D. T. Valenta, Y. Altman, S. Harvey, H. Xie, S. Mitragotri, J. W. Smith, Polymer particle shape independently influences binding and internalization by macrophages. *J. Control. Release* **147**, 408–412 (2010).
31. A. Lejeune, P. Poyet, R. C. Gaudreault, C. Gicquaud, Nanoerythrosomes, a new derivative of erythrocyte ghost: III. Is phagocytosis involved in the mechanism of action? *Anticancer Res* **17**, 3599–3603 (1997).
32. C.-M. J. Hu, R. H. Fang, J. Copp, B. T. Luk, L. Zhang, A biomimetic nanosponge that absorbs pore-forming toxins. *Nat. Nanotechnol.* **8**, 336–340 (2013).
33. J. C. Sunshine, K. Perica, J. P. Schneck, J. J. Green, Particle shape dependence of CD8+ T cell activation by artificial antigen presenting cells. *Biomaterials* **35**, 269–277 (2014).
34. K. W. von Appen, D. Weber, U. Losert, H. Schima, H. J. Gurland, D. Falkenhagen, Microspheres based detoxification system: A new method in convective blood purification. *Artif. Organs* **20**, 420–425 (1996).
35. R. A. Meyer, M. P. Mathew, E. Ben-Akiva, J. C. Sunshine, R. B. Shmueli, Q. Ren, K. J. Yarema, J. J. Green, Anisotropic biodegradable lipid coated particles for spatially dynamic protein presentation. *Acta Biomater.* **72**, 228–238 (2018).
36. J. C. Black, P. P. Cheney, T. Campbell, M. K. Knowles, Membrane curvature based lipid sorting using a nanoparticle patterned substrate. *Soft Matter* **10**, 2016–2023 (2014).
37. E. Ben-Akiva, K. R. Rhodes, R. A. Meyer, J. J. Green, Fabrication of anisotropic polymeric artificial antigen presenting cells for $CD8^+$ T cell activation. *J. Vis. Exp.*, e58332 (2018).
38. J. A. Champion, Y. K. Katare, S. Mitragotri, Making polymeric micro- and nanoparticles of complex shapes. *Proc. Natl. Acad. Sci. U.S.A.* **104**, 11901–11904 (2007).

Acknowledgments: We thank M. McCaffery and the Johns Hopkins University Integrated Imaging Center for assistance with TEM imaging. **Funding:** E.B.-A. (DGE-1746891) thanks the NSF for a Graduate Research Fellowship, and we thank the NIH for support (R01EB022148 and R01CA228133). R.A.M. thanks the Achievement Rewards for College Scientists (ARCS) and the National Cancer Institute of the NIH (F31CA214147) for fellowship support. We also thank the Bloomberg~Kimmel Institute for Cancer Immunotherapy for support. **Author contributions:** E.B.-A., R.A.M., and J.J.G. conceived and designed the

research. E.B.-A., H.Y., J.T.S., and R.A.M. performed experiments. E.B.-A. analyzed the data and performed statistical analysis. D.M.P. and J.J.G. provided resources and funding acquisition. E.B.-A., R.A.M., D.M.P., and J.J.G. wrote and edited the paper. D.M.P. and J.J.G. provided supervision and administration. All authors approved the paper. **Competing interests:** The authors declare that they have no competing interests. **Data and materials availability:** All data needed to evaluate the conclusions in the paper are present in the paper and/or the Supplementary Materials. Additional data related to this paper may be requested from the authors.

Submitted 30 July 2019
Accepted 22 January 2020
Published 15 April 2020
10.1126/sciadv.aay9035

Citation: E. Ben-Akiva, R. A. Meyer, H. Yu, J. T. Smith, D. M. Pardoll, J. J. Green, Biomimetic anisotropic polymeric nanoparticles coated with red blood cell membranes for enhanced circulation and toxin removal. *Sci. Adv.* **6**, eaay9035 (2020).